Synthesis of Crystalline Micron Spheres of Titanium Dioxide by Thermal Plasma Oxidation of Titanium Carbide

Ya-Li Li and Takamasa Ishigaki*

National Institute for Materials Science, Tsukuba, Ibaraki 305-0044, Japan

Received November 14, 2000. Revised Manuscript Received January 22, 2001

Spherical micron particles of crystalline titanium dioxide (TiO_2) were synthesized by in-flight oxidation of titanium carbide (TiC) micron powders (mean diameter: 28 μm) in argon−oxygen thermal plasma. The extent of oxidation of TiC powders increases with the flow rate of oxygen in the plasma gases (Ar + O_2), and a nearly complete oxidation was achieved at a higher oxygen input (10 L/min) yielding TiO_2 powders as the oxidized product. Morphology examination showed that the particles generated by this process are monodispersed and are perfectly spherical. Particle sizes of the as-produced powders range from submicron to several tens of micrometers and are characterized by a bimodal size distribution. A simple sedimentation treatment was applied to separate the as-formed powders with alcohol solvent to give uniform spherical particles with monomodal size distributions. Microstructure analysis of individual particle by aid of selected area Raman spectrum revealed that all the spherical particles are totally crystalline, comprised of either rutile or anatase or their composite. The formation mechanism of the TiO_2 particles in the plasma oxidation was discussed.

I. Introduction

Titanium oxides (TiO_2) have a variety of functional applications ranging from pigments to photoconductors to sensor materials to dielectric ceramics.[1,2] The materials have also been studied extensively in recent years as photocatalysts,[3] ceramic members,[4] and nanostructured ceramics.[5] For most of these applications, monodispersed spherical TiO_2 particles are desired because they usually give improved properties in the respective applications. Examples are that monodispersed spherical particles give a high compaction density in ceramic processing[6] and a dense array in deposited film.[7] Moreover, control of particle size and crystallinity of the TiO_2 powders are critical to their functional applications. It is known that only crystalline TiO_2 (both rutile and anatase) possesses effective light scattering, and the efficiency of light scattering attains the maximum when particle diameters are in submicron sizes.[8] Also, crystalline TiO_2 exhibits effective photocatalysts, while amorphous TiO_2 does not.[9] From a practical point of view, larger spherical and crystalline TiO_2 powders (submicron or micron size) are desired for the photocatalyst application since they provide good behavior of separation from the processed materials, which is not exhibited by the currently utilized nanosize powders.[10] Thus, synthesis of highly crystallized spherical TiO_2 particles has great technical interests.

Although many methods have been developed to synthesize TiO_2 powders,[7,11−19] there are still limitations to producing high-quality spherical crystalline TiO_2 particles by the existing synthesis techniques. Industrial methods to produce commercial TiO_2 powders are based on the so-called "sulfate" process and "chloride".[11,12] The TiO_2 particles produced by these processes are usually not in spherical shapes.[11,12] Other methods developed in recent years are mainly based on the aerosol pyrolysis and alkyloxide hydrolysis in use of different kinds of alkyloxide or other titanium-containing compounds.[13−19] Along the route of alkyloxide hydrolysis, well-defined

* To whom correspondence should be addressed: Advanced Materials Laboratory, National Institute for Materials Science, Tsukuba, Ibaraki 305-0044, Japan. Fax: +81-298-514005. Tel.: +81-298-513351. E-mail: ISHIGAKI.Takamasa@nims.go.jp.

(1) Kingery, W. D.; Bowen, H. K.; Uhlmann, D. R. *Introduction to Ceramics*; John Wiley & Sons: New York, 1976.
(2) Hench, L. L.; Ulrich, D. R. *Ultrastructure Processing of Ceramics, Glasses, and Composites*; John Wiley & Sons: New York, 1984.
(3) Ollis, D. F.; Al-Ekabi, H. *Photocatalytic Purification and Treatment of Water and Air*; Elsevier: Amsterdam, 1993.
(4) Kumar, O.; Keizer, K.; Burgraff, A. J. *J. Mater. Chem.* **1993**, *3*, 1141.
(5) Kumar, K. P.; Keizer, K.; Burggraaf, A. J.; Okubo, T.; Nagamoto, H.; Morooka, S. *Nature* **1992**, *358*, 48.
(6) Barringer, E. A.;. Bowen, H. K. *J. Am. Ceram. Soc.* **1982**, *65*, C-199.
(7) Burnside, S. D.; Shklover, V.; Barbe, C.; Comte, P.; Arendse, F.; Brooks, K.; Gratzel, M. *Chem. Mater.* **1998**, *10*, 2419.
(8) Mayers, P. R.; Long, J. S. *Treatise on Coatings, Vol. 3, Pigments;* Marcel Dekker: New York, 1977; p 479.
(9) Ohtani, B.; Ogawa, Y.; Nishimoto, S. I. *J. Phys. Chem.* **1997**, *B101*, 3746.
(10) Loddo, V.; Marci, G.; Martin, C.; Palmisano, L.; Rives, V.; Scafani, A. *Appl. Catal. B* **1999**, *20*, 29.
(11) Pratsinis, S. E.; Vemury, S. *Powder Technol.* **1996**, *88*, 267.
(12) Visca, M.; Matijevic, E. *J. Colloid Interface Sci.* **1979**, *68*, 308.
(13) Matijevic, E.; Budnik, M.; Meites, L. *J. Colloid Interface Sci.* **1977**, *61*, 302.
(14) Fegley, B.; Barringer, E. A.; Bowen, H. K. *J. Am. Ceram. Soc.* **1984**, *67*, C-113.
(15) Jean, J.; Ring, T. A. *Am. Ceram. Soc. Bull.* **1986**, *65*, 1574.
(16) Park, H. K.; Moon, Y. T.; Kim, D. K.; Kim, C. H. *J. Am. Ceram. Soc.* **1996**, *79*, 2727.
(17) Ahonen, P. P.; Kauppinen, E. I.; Joubert, J. C.; Deschanvres, J. L.; Tendeloo, G. V. *J. Mater. Res.* **1999**, *14*, 3938.
(18) Akhtar, M. K.; Pratsinis, S. E.; Mastrangelo, S. V. R. *J. Am. Ceram. Soc.* **1992**, *75*, 3408.
(19) Ayllon, J. A.; Figueras, A.; Garelik, S.; Spirkova, L.; Durand, J.; Cot, L. *J. Mater. Sci. Lett.* **1999**, *18*, 1319.

10.1021/cm000893u CCC: $20.00
Published on Web 03/20/2001

spherical particles can be obtained.[6,13−15] Unfortunately, the as-synthesized particles by this process are usually amorphous or poorly crystallized [6,12−14] because of the low synthesis temperature (<100 °C) in this wet chemical route.[6,13] In the flame-heating aerosol reactions, doping $POCl_3$, $SiCl_4$, and BCl_3 into $TiCl_4$ (1−10 mol ratio to $TiCl_4$) was investigated to alter the morphology of the titania particles from polyhedral to spheroidal (0.1 μm);[18] however, the spherical particles produced are also amorphous.

Numerous works report on the crystallization of amorphous particles to crystallized ones either by improvement in the synthesis process or by subsequent processing, such as hydrothermal treatment,[20−22] aging of the sol or gel precursor of TiO_2,[23] and by routine high-temperature annealing of hydrolysis-derived amorphous powders.[17,24,25] However, these additional treatments commonly resulted in particle aggregation[20] and/or irregular grain growth.[20,21,23−25]

In the present work, we report on a high-temperature process capable of producing highly crystallized and monodispersed spherical TiO_2 particles at the submicron to micron size scale. This process is based on induction thermal plasma oxidation of in-flight refractory titanium carbide micron powders. Induction thermal plasma treatment of in-flight refractory solid particles is characterized by its extreme high-heating temperature (5 000−10 000 K) and, correspondingly, very high heating and cooling rate ($\sim 10^6$ K/min) for the rapidly moving particles during processing,[26] which has been successfully applied to the generation of spherical particles of several refractory ceramics through a rapid solidification from partially or complete melting of the refractory particles[27−30] In the present investigation to synthesize TiO_2, TiC being adopted as the precursor of TiO_2 is partially due to the fact that it is refractory and is meltable (melting point: 3140 °C), which are desired for the thermal plasma synthesis to generate spherical particles. A thermodynamic equilibrium calculation in the TiC(s) + O_2 system indicates that TiO_2 is thermodynamically favored in a wide range of temperatures. It is expected that by injection of TiC micron powders into argon−oxygen induction thermal plasma, rapid melting and oxidation of the TiC micron particles seem to yield TiO_2 particles.

II. Experimental Section

Experiments of plasma oxidation of TiC powders was conducted on a powder synthesis reactor equipped with induction plasma with the operation energy level between 15 and 40 kW. One advantage of the induction plasma is that oxygen can be mixed in as plasma-generating gas, which allows oxidation processing of materials in the plasma high-temperature region. Such oxidation processing is essentially limited in the common direct current (dc) arc plasma-based process wherein introduction of oxygen gas in plasma would oxidize the anode materials.

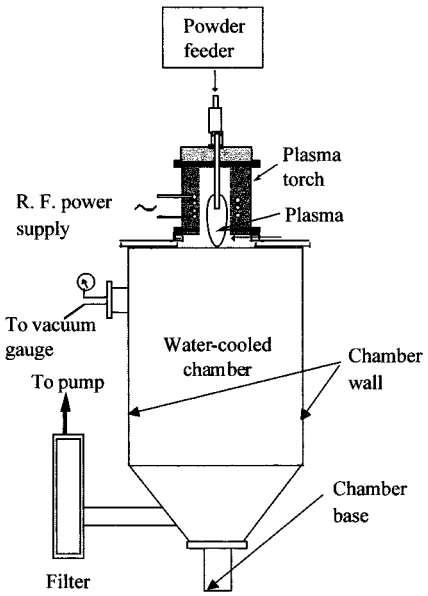

Figure 1. Schematic illustration of the principle of plasma processing of in-flight solid particles.

Table 1. Experimental Conditions for In-Flight Plasma Oxidation of TiC

parameter	value
sheath gas and flow rate	total (argon + oxygen), 90 L/min; oxygen, 2.5−10 L/min
center gas and flow rate (Φ)	argon, 30 L/min
carrier gas and flow rate (Φ_c)	argon, 5 L/min
powder feeding rate (R_F)	0.8−4 g/min
inductive power (P)	25 kW
reactor pressure (p)	66.7 kPa

In the present work, the high-temperature thermal plasma was generated by an induction-plasma torch (model PL 50, TEKNA Plasma Systems, Sherbrooke, Quebec, Canada) connected with a radio frequency (rf) power-supply system (2 MHz, Nihon Koshuha Co. Ltd., Yokohama, Kanagawa, Japan). The starting TiC powders utilized were a commercial product (TiC-M, Nippon New Metal, Osaka, Japan), which have a mean diameter of 28 μm and a composition of $TiC_{0.97}$. The oxygen content in the TiC powders was determined to be 0.29 wt %.

Figure 1 shows a schematic illustration of the plasma-assisted in-flight treatment of refractory solid particles employed in this study. In this process, TiC particles were axially injected from the top of the plasma torch into the center of the plasma region by a powder feeder using argon as a carrier. For the oxidation treatment, high-purity oxygen (99.99 wt %) was mixed with argon (purity: 99.99 wt %) in a different ratio and was injected from the top of the torch as plasma sheath gas. Synthesis conditions for the plasma oxidation treatment are listed in Table 1.

Oxidized products from the plasma treatment were collected from the wall and bottom of the reactor chamber. The received powders were characterized in terms of morphology, microstructure, and particle size distributions. Unless specified, the powders characterized were collected from chamber walls where the major part of the oxidized products located (> 95 wt %). The particle morphology was examined by optical microscopy and scanning electronic microscopy (SEM) (model

(20) Bacsa, R. R.; Gratzel, M. *J. Am. Ceram. Soc.* **1996**, *79*, 2185.
(21) Ovenstone, J.; Yanagisawa, K. *Chem. Mater.* **1999**, *11*, 2770.
(22) Wang, C. C.; Ying, J. Y. *Chem. Mater.* **1999**, *11*, 3113.
(23) Slunecko, J.; Kosec, M.; Holc, J.; Drazic, G. *J. Am. Ceram. Soc.* **1998**, *81*, 1121.
(24) Ocana, M.; Ramos, J. V.; Serna, C. J. *J. Am. Ceram. Soc.* **1992**, *75*, 2010.
(25) Edelson, L. H.; Glaeser, A. M. *J. Am. Ceram. Soc.* **1988**, *71*, C-198.
(26) Boulos, M. I.; Fauchaus, P.; Pfender, E. *Thermal Plasma Vol 1*; Plenum Press: New York, 1994.
(27) Ishigaki, T.; Jurewicz, J.; Tanaka, J.; Moriyoshi, Y.; Boulos, M. I. *J. Mater. Sci.* **1995**, *30*, 883.
(28) Ishigaki, T.; Moriyoshi, Y.; Watanabe, T.; Kanzawa, A. *J. Mater. Res.* **1996**, *11*, 2811.
(29) Fan, X.; Ishigaki, T.; Sato, Y. *J. Am. Ceram. Soc.* **1999**, *82*, 281.
(30) Fan, X.; Ishigaki, T.; Sato, Y., *J. Mater. Res.* **1997**, *12*, 1315; **1996**, *11*, 2598.

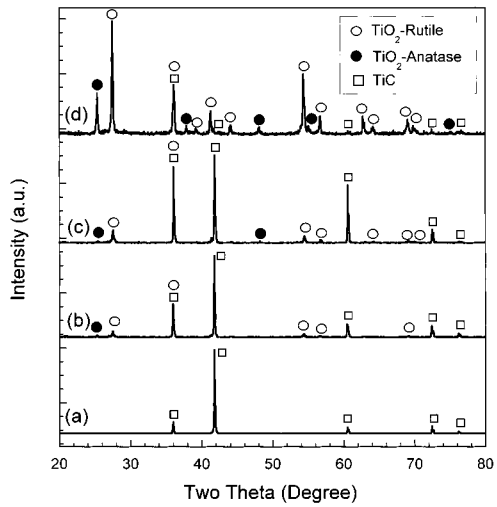

Figure 2. X-ray diffractions of the oxidized products formed by $Ar-O_2$ plasma oxidation of TiC powders under different oxygen input: (a) the starting TiC powders; (b) after $Ar-O_2$ plasma treatment at oxygen flow rate, $\Phi_{O_2} = 2.5$ L/min; (c) $\Phi_{O_2} = 5$ L/min; (d) $\Phi_{O_2} = 10$ L/min.

S-5000, Hitachi, Tokyo, Japan). Particle size distribution was measured by the method of laser scattering (Sympatec HELOS & RODOS laser diffraction analyzer, Germany). X-ray powder diffraction (XRD) was performed with Cu Kα radiation. Phase contents of the TiO_2 phases and TiC residue in the oxidized products were determined according to the intensities of the diffraction lines: (101) for anatase, (110) for rutile, and (100) for TiC, using alumina as an internal calibrate. To investigate the internal structure of the produced TiO_2 particles, powder products were embedded in an organic resin and were polished to expose the cross section of the TiO_2 particles. The cross sections of TiO_2 particles were analyzed by micron Raman spectroscopy (Raman Spectroscopy, NR-1800, JASCO Japan) under Ar^+ laser excitation with laser energy of 100 mW and a detection spot of ~1 μm in diameter.

III. Results

III.1. Formation of Crystalline TiO_2 Spheres. After $Ar-O_2$ plasma processing, fluffy powders of oxidized products were collected from the chamber wall and base. The oxidized products change in color from gray, dark green, to white, depending on the extent of oxidation of the TiC or processing conditions. The appearance of the obtained products is different from that of the initial TiC powders, which are dark and lustrous, a result of oxidation reactions.

Figure 2 shows X-ray diffraction (XRD) patterns of several oxidized products that were obtained at different flow rates of oxygen in the plasma gases ($Ar + O_2$). Formation of TiO_2 phases in the oxidized products is evident from their strong diffraction lines that correspond to the rutile and anatase structure, the two modifications of TiO_2. With the increase of oxygen flow rate from 2.5 to 10 L/min, the diffraction lines for TiO_2 (both rutile and anatase) increase distinctly in intensity relative to those of TiC, suggesting the increased extent of oxidation as the oxygen concentration in the plasma reaction zone increases. X-ray diffraction of the oxidized products formed at an oxygen flow rate (Φ_{O_2}) of 10 L/min shows mainly the diffraction lines of TiO_2 (rutile and anatase) with only weak signals of TiC. Quantitative phase analysis indicates that the TiC residue was 0.6 wt % in the oxidized products formed under this condition.

Morphologies of the TiO_2 powders produced by plasma oxidation were examined by optical microscopy, as shown in Figure 3, in which the morphology of the starting TiC particles is also included for comparison. In contrast to the starting irregularly shaped TiC particles (Figure 3a), well-defined spherical particles were formed after the plasma oxidization treatment (Figure 3b,c). Under reflection optical microscopy, the TiO_2 particles exhibit red or green colors, owing to their unique refraction in visible light. The TiO_2 particles can be distinguished visibly from the unreacted or partly oxidized TiC particles in incomplete oxidized products that appear as dark particles under reflection light optical microscopy observation; for instance, the dark TiC particles in Figure 4c are the unoxidized but spheroidized TiC after the plasma processing.

The morphologies of as-synthesized particles are somewhat different for the powders collected at different areas in the reaction chamber. Spherical particles with the "clean" surfaces, like those shown in Figure 3b,c, were obtained mainly from the base of the reactor chamber. Also, the particles aggregated in this area have larger sizes (24−30 μm). The wall-deposits that occupy 80−90 vol % of the total oxidized products are found, however, to be a mixture of the spherical TiO_2 particles and the fine nanosize deposits (Figure 3d), the latter sticking on the surface of the larger spherical particles, making the perimeters of the micron-size spheres faint under optical microscopy observation.

Figure 4 shows SEM morphology of several as-formed particles in the wall-collected powders of the complete oxidation product, with the fine deposit on the surface of the micron spherical particles. Enlarged magnification revealed that the fine particles are equaxial with a uniform diameter in the range of 30−50 nm (Figure 4b). The fine deposits, as commonly found in thermal plasma treatment of other refractories, is a product of direct condensation from the vapor phase, which occurred partially in the present process, in addition to the process of the melt−solidification, which produces the spherical particle.

Particle size distributions of as-produced TiO_2 powders obtained under complete oxidation conditions were measured by laser diffraction, as shown in Figure 5, in which the size distribution curve for the starting TiC powders is also included for comparison. The starting TiC powders exhibit a narrow size distribution of log-normal style with a geometric standard deviation of $\sigma_g = 1.67$. After the oxidation treatment in $Ar-O_2$ plasma, the oxidized products display a bimodal size distribution with a wide spread in particle diameters ranging from 0.05 to 30 μm. The small size particles are in the range of 0.05−10 μm in diameter with a mean diameter (d_{50}) of 2.1 μm, determined from the cumulative curve. This mean size is much smaller than the starting TiC particle size (mean diameter: 28 μm), suggesting that oxidization of TiC occurs through decomposition of the bigger TiC particles in the plasma during oxidation treatment. The other portion in the oxidized products is the bigger TiO_2 particles, which have a mean diameter of 24 μm, which is slightly smaller than the particle size in the original TiC powders (28 μm). The existence of abundant bigger TiO_2 particles in the oxidized products have already been confirmed by optical microscopy observa-

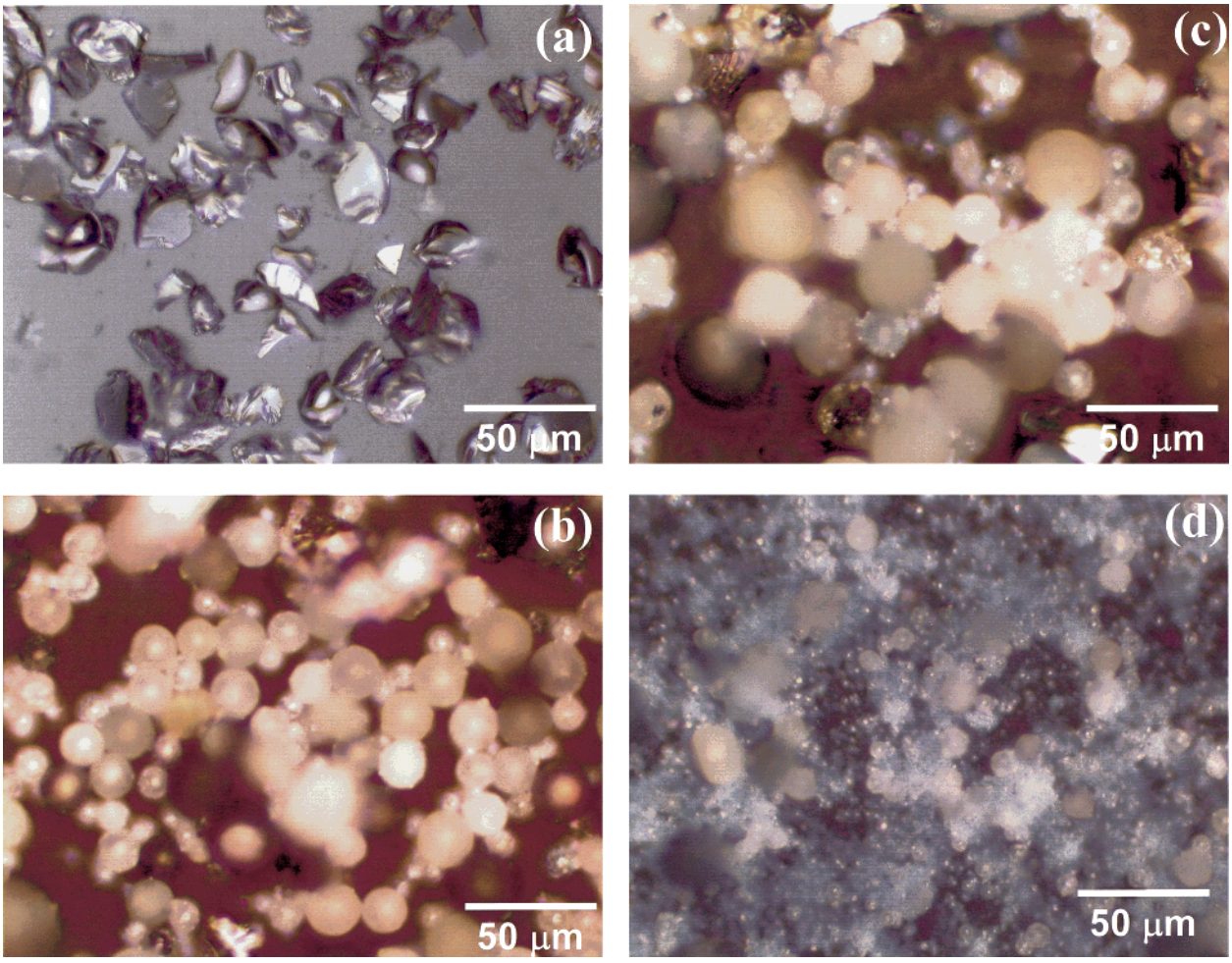

Figure 3. Morphology of as-oxidized powders by Ar−O_2 plasma oxidation of TiC: (a) unprocessed TiC particles; (b),(c) TiO_2 particles collected from the bottom portion of the reactor chamber which were formed at $\Phi_{O_2} = 10$ L/min (b) and $\Phi_{O_2} = 5$ L/min (c); and (d) TiO_2 powders collected from the chamber wall, which were synthesized at $\Phi_{O_2} = 10$ L/min. Other synthesis parameters are $P = 25$ kW, $\Phi_c = 5$ L/min, $R_F = 1.83$ g/min, and $p = 66.7$ kPa.

tion (Figure 3). The formation of the bigger TiO_2 particles with an independent size distribution in oxidized products implies that they were formed by a different mechanism from that for the smaller size particles.

III.2. Sedimentation Separation. The as-produced TiO_2 powders after plasma synthesis are a mixture of monodispersed micron and submicron spheres of TiO_2, and the vapor-condensed nanosize particles in completely oxidized products, together with the unoxidized TiC particles in the incomplete oxidized products. The different constituents in the as-synthesized products can be separated easily from their mixture by performing a simple sedimentation treatment using common alcoholic solvents.

We dispersed the wall powders of a completely oxidized product (10 vol %) in pure ethanol (99.99 wt %), and the suspension was then dispersed by assistance of ultrasonic vibrations. By control of the sedimentation time, the two types of particles in the oxidized product (the smaller particles with $d_{50} = 2.1$ μm and the bigger ones $d_{50} = 24$ μm) have been successfully separated. Figures 6 and 7 show the morphologies of the bigger size and the smaller size particles obtained from the same batch of powders, respectively. It is evident that all the bigger particles (>10 μm) are removed by the sedimentation process (Figure 7). A small number of unoxidized TiC particles were left in the bigger size particles (the irregular particles in Figure 6), which could be removed by further sediment treatment. After the separation treatment, each type of the obtained powders exhibit a monomodal distribution as shown by particle size distributions in Figure 8. Depending on the extent of oxidation, powder yield with respect to the starting TiC powders was in the range of 30−60 wt % for the bigger size particles after sedimentation treatment.

III.3. Morphology and Structure of Individual Particles. Figure 9 shows typical surface morphologies of the TiO_2 micron spheres synthesized by the plasma oxidation. Most of the particles have a smooth surface like the one shown in Figure 9a, in particular, for particles with smaller diameters. Particles with a rough surface consisting of irregular convex lines are frequently observed in moderate and larger size particles (Figure 9b). The rough surface with convex lines is an indicator of incomplete liquid diffusion of TiO_2 droplets during particle formation. Besides, particles with ditches or concaves on their surfaces are sporadically observable (Figure 9c,d). These particle structures are reminiscent of a coalescence growth of smaller droplets and are a result of the rapid quenching before the completion of the coalescence or sintering. SEM examination shows that all the particles are monodispersed without surface

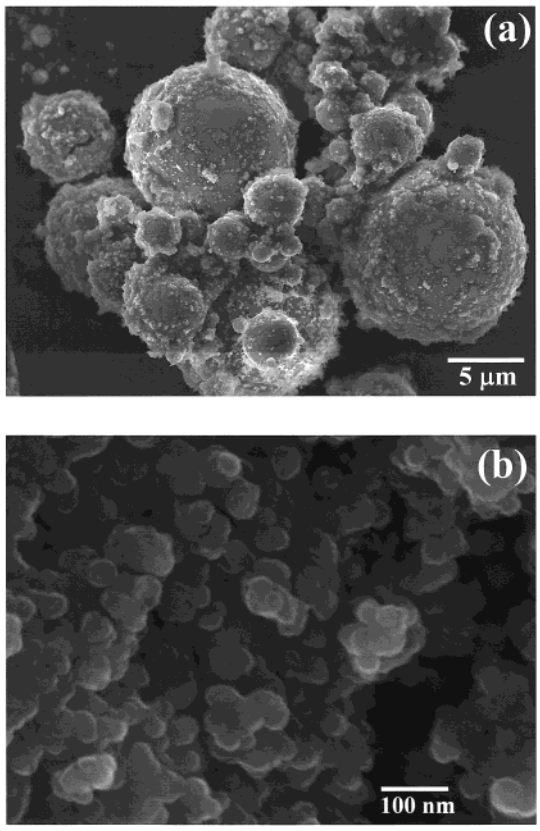

Figure 4. SEM morphology of as-synthesized TiO_2 spheres. The powders were collected from the wall portion in the reaction chamber. (a) shows the as-synthesized micro TiO_2 spheres with many fine deposits on particle surfaces; and (b) is an enlarged image of the surface deposits, revealing the nanosize particles being around 30−50 nm in diameter.

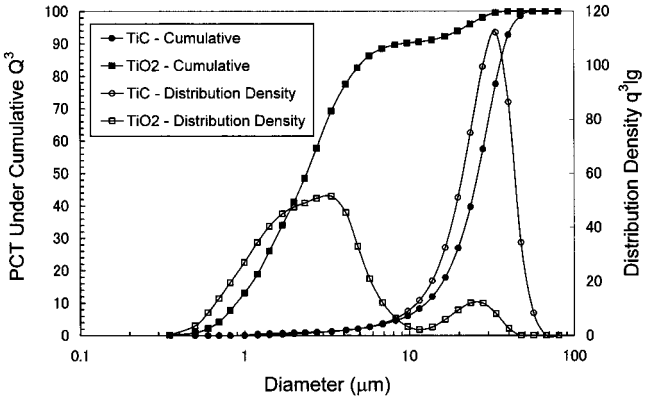

Figure 5. Particle size distribution of the starting TiC powders (a) and the TiO_2 powders produced by plasma oxidation of TiC (b). The TiO_2 powders were formed under complete oxidation conditions: $\Phi_{O_2} = 10$ L/min, $P = 25$ kW, $\Phi_c = 5$ L/min, $R_F = 1.0$ g/min, and $p = 66.7$ kPa.

sintering, indicating rapid coagulation kinetics under the high-temperature plasma heating.

The internal structure of TiO_2 spheres was examined by microstructure observation of their cross sections revealed by polishing the particles embedded in organic resin. All of the micron size TiO_2 spheres are found to be fully dense, like those shown in Figure 10 a. However, some hollow particles were also observed in bigger size particles like the one shown in Figure 11.

Figure 10b shows Raman spectra acquired on the cross section of the micron spheres in Figure 10a. All

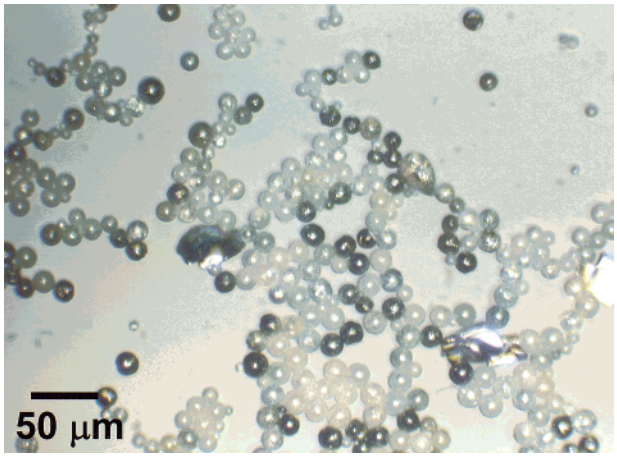

Figure 6. Optical microscopy morphologies of the bigger size TiO_2 particles obtained by alcohol-solvent sedimentation separation of as-produced TiO_2 powders by plasma oxidation.

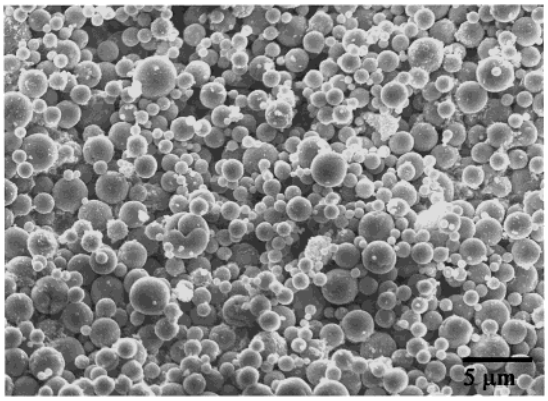

Figure 7. SEM morphology of the smaller size TiO_2 powders separated from the as-produced powders by sedimentation treatment using alcohol solvents.

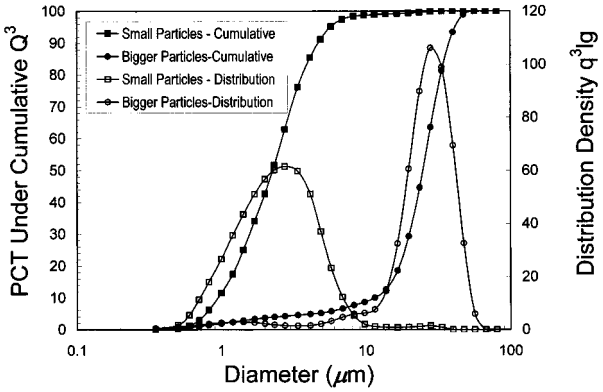

Figure 8. Particle size distribution of the two differently sized particles obtained by the sedimentation treatment using alcohol solvents. The raw TiO_2 powders were synthesized at an oxygen flow rate of 10 L/min.

the particles formed under complete oxidization conditions were identified to be entirely crystalline TiO_2. The phases detected from the cross sections of the various size particles are either monolithic rutile, anatase, or a mixture of the two modifications. Selected area detection on the cross section of individual particles revealed that, in anatase−rutile two-phase particles, the rutile distributes at the outer layer of the spheres while the inner part is pure anatase, as evident from the Raman spectrum collected from the different regions in particle

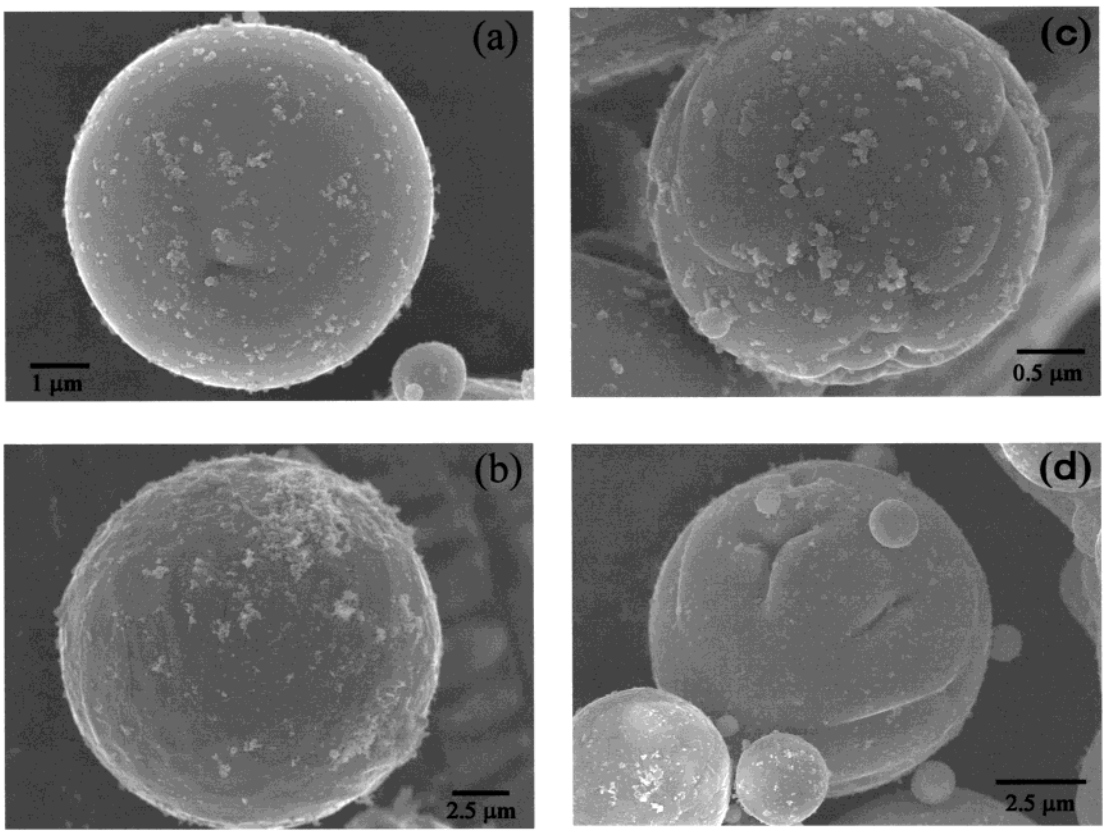

Figure 9. Various surface morphologies of the TiO_2 micron spheres produced by $Ar-O_2$ plasma oxidation. (a) Particles with a smooth surface; (b) rough surface with strip convexes; (c),(d) particles with surface trenches showing incomplete coalescence of smaller primary particles.

A. This phase structure is likely to result from an incomplete transformation of anatase to rutile that started at the outer surface of the initially solidified anatase particle. For the monolith anatase and rutile particle, the phase distributes quite uniform inside particles. (e.g., particles E and D in Figure 10). Also, no amorphous structure was found inside TiO_2 spheres in a number of particles examined, suggesting the high degree of crystallization of the TiO_2 spheres generated by this novel process.

IV. Discussion

Study demonstrates that thermal-plasma oxidation of TiC can generate monodispersed TiO_2 micron spheres of highly crystallized characteristics. The formation of well-defined crystalline spheres benefits from the extremely high synthesis temperature in the induction thermal plasma (>3 000−10 000 K), which allows rapid oxidation of TiC followed by generation of low-viscosity TiO_2 droplets and the very high cooling rate (10^6 K/s) that allows rapid solidification of the melt droplets to form unagglomerated spheres.

The TiO_2 particles produced in the present process exhibit typically a bimodal size distribution (Figure 5). This implies the existence of different mechanisms for the formation of the two differently sized particles. The small size spheres with a mean diameter of $d_{50} \sim 2.1$ μm, far less than the starting TiC particles (mean diameter of $d_{50} \sim 28$ μm), suggest that they were formed by disintegration of the bigger TiC particles during the oxidation reaction. Figure 11 shows an as-formed big hollow particle settled in with smaller spheres, which is believed to represent the major mechanism for the formation of the small spherical particles. This morphology demonstrates that the small TiO_2 particles were generated simultaneously with local oxidation depletion of the original TiC particle. The locally preferential depletion of TiC particles is probably related to the strong exothermal oxidation reaction between TiC and O_2 ($TiC(L) + {}^3/_2O_2(g) = TiO_2(L) + CO(g)$, $\Delta H = -1050$ kJ/mol), which provides extensive heat for further melting of solid TiC at the oxidation front, which macroscopically exhibits as a propagation oxidation reaction once melting and oxidation of the TiC were initiated. The rapid oxidation inside or surrounding TiC particles generates locally highly concentrated TiO_2 droplets or vapor that condense or coagulate to give monodispersed micron spheres. The particle size depends on the local oxidation rate or the degree of supersaturation of TiO_2 vapors or reactive species.

The bigger TiO_2 particles that coexisted with the smaller particles in the fully oxidized product are likely to be formed from direct oxidation of TiC particles after melting. For complete oxidation, the formation of the less denser crystalline TiO_2 (density 4.8 g/cm^3) from the denser TiC (6.5 g/cm^3) involves a volume increase by a factor of 1.8. This gives a mean particle diameter of 34 μm for the TiO_2 particles that are from the starting TiC with a diameter of 28 μm, provided that the melting and oxidation occurred in individual particles. However, the diameter of the bigger particles observed in the oxidized products ($d_{50} = 24$ μm) is smaller than what should be under entire oxidation of individual TiC particles. This

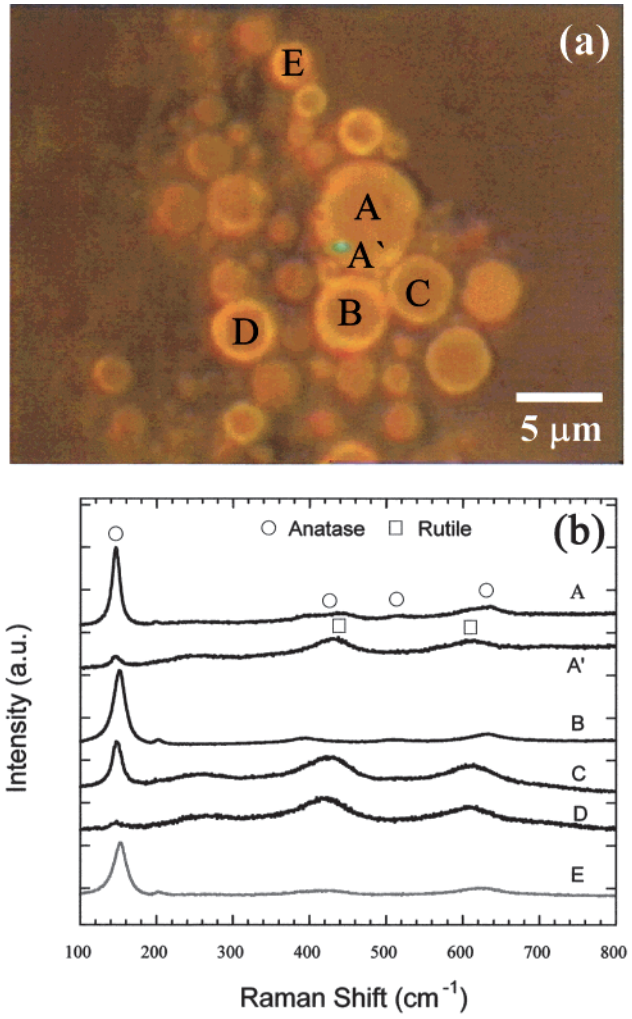

Figure 10. Raman analyses of cross sections of TiO_2 particles. (a) Sectioned TiO_2 particles prepared by polish of embedded TiO_2 particles in organic resins; (b) the corresponding Raman spectra acquired from the cross section of the TiO_2 particles shown in (a). Spectrum A in (b) corresponds to the center area of particle A in (a), and spectrum A` corresponds to the periphery of particle A, i.e., area A` in particle A. The bright spot labeled with A` is the actual spot of the Ar^+ laser incident beam for the Raman excitation.

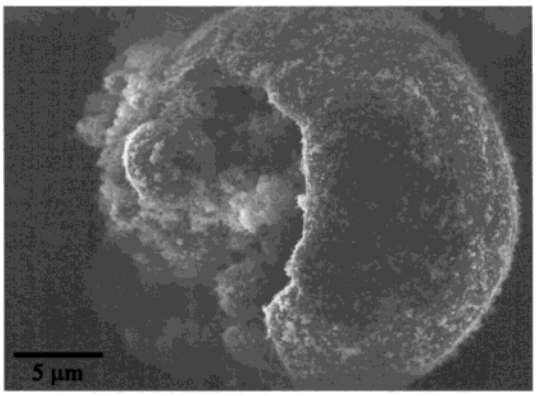

Figure 11. An as-formed hollow TiO_2 particle settled in with smaller TiO_2 particles that were generated by a local oxidation depletion of TiC particle during plasma oxidation treatment. The hollow TiO_2 particle was oxidized entirely in the liquid phase after the partially depleted TiC totally melted.

difference may arise from the initial partial evaporation of TiC particles prior to oxidation or subsequent evaporation of the TiO_2 droplets during their residence in the high-temperature region after oxidation reaction.

Partial depletion of TiC by local oxidation is another possible origination of the relatively smaller diameters of the big TiO_2 particles. As TiC particles were injected into the high-temperature zone of thermal plasma, the particles were initially oxidized in an area where melting was initiated, and subsequently, the residual main part of TiC melted entirely and was oxidized totally, followed by a spheroidization of the hollow part of TiO_2 accompanied by a shrinkage in apparent dimension. The morphology of the particles given in Figure 11 provides evidence of the occurrence of the entire oxidation of partially depleted TiC prior to spheroidization (the hollow particle in Figure 11 was identified to be TiO_2 (rutile)). It is reasonable to deduce that if the particle stayed in the high-temperature region longer, it would spheroidize to form a spherical TiO_2 particle with a smaller size than the hollow particle.

In a vapor or liquid process via pyrolysis of chloride titanium or other alkyloxide precursors, the decomposition of the reactant is rapid and the nucleation and growth of TiO_2 particles occur in a quasi-equilibrium state after the completion of chemical reactions; thus, the final particles have a narrow size distribution and conform to the log-normal style, which is a reflection of collision−growth of primary particles governed by Brownian coagulation.[11,31] What is different in the present process via oxidation of refractory TiC is that the nucleation and growth of TiO_2 particles occur continuously with the oxidation of TiC until the particles arrive in the region where the temperature is low enough to cease the reaction. The nucleation and growth of TiO_2 particles occur either from the newly produced species from the continuous oxidation or coalescence of primary particles or from the already formed droplets as already evident from the microstructure observation (Figure 9).

The heterogeneous distribution of the TiO_2 powders with different morphologies and diameters in the reaction chamber (Figure 3) are related to the different trajectories and the associated heating and reaction histories for the individual TiC particle in the plasma zone during the oxidation treatment. The replacement oxidation of TiC particles occurs predominately in the plasma center region along the main axial of reactant flow where it is relatively wild in temperature and has longer residue time,[32] thus favorable for melting of TiC and inducing oxidation in the liquid phase. This explains the accumulation of a high ratio of bigger TiO_2 particles with less surface deposit in the bottom area in the plasma synthesis chamber. Impeded depletion oxidation reaction in vapor occurred predominately in areas near end induction coils where the high-temperature region is located,[32] thus producing smaller particles and a fine deposit around the wall portion of the reaction chamber.

Increasing the flow rate of oxygen in plasma gases impedes the oxidation reaction and at the same time provides more heat for further melting and oxidation of the residue TiC, thus enhancing the conversion of TiC to TiO_2 as observed experimentally (Figure 2). Especially, vapor phase oxidation is greatly enhanced at high

(31) Kusters, K. A.; Pratsnis, S. E. *Powder Technol.* **1991**, *82*, 79.
(32) Chen, K.; Boulos, M. I. *J. Phys. D: Appl. Phys.* **1994**, *27*, 946−952.

oxygen potential. This is evident from the experimental observation that the fraction of smaller particles increases distinctly with oxygen input, and as the oxygen flow rate was increased up to 20 L/min, the oxidized products contain only the vapor condensed fine particles and smaller spheres. On the other hand, when oxygen input is low (<10 L/min), the fraction of big particles increases (50−70 wt %), indicating the prevalence of liquid oxidation. However, the low oxygen input cannot ensure complete oxidation of all the TiC particles, which may result in partially oxidized or unoxidized particles in products. A moderate oxygen flow rate seems to be necessary to depress over evaporation and simultaneously ensure the at-most oxidation of TiC. The optimal oxygen flow rate was found to be around 10 L/min in the present experimental conditions for producing a high ratio of TiO_2 spheres.

Acknowledgment. Science and Technology Agency of Japanese Government is greatly acknowledged for granting a research fellowship for Y. Li. We thank Mr. K. Kosuda for his assistance in performing SEM experiments and Dr. K. Watanabe for his help with Raman spectral measurements.

CM000893U